Applied Energy (2018), 228, 1953-1965.

FUEL UTILIZATION EFFECTS ON SYSTEM EFFICIENCY IN SOLID OXIDE FUEL CELL GAS TURBINE HYBRID SYSTEMS

Danylo Oryshchyn, Nor Farida Harun, David Tucker, M. Kenneth Bryden*, Lawrence Shadle[1]

U.S. Department of Energy, National Energy Technology Laboratory,

3610 Collins Ferry Rd. Morgantown, WV 26507, United States

* Simulation and Decision Science Program, Ames Laboratory, Ames, IA 50011, United States

ABSTRACT

A computational analysis was conducted to optimize the design of a solid oxide fuel cell - gas turbine hybrid power generator, focusing on the impact that fuel utilization within the fuel cell has on system efficiency and installed costs. This is the first ever design-study considering the effect of fuel utilization on performance, as well as on the optimum power split. This hybrid system attained high electric generation efficiencies (>70%) over a wide range of operating conditions (60%< fuel utilization <90%) while the fuel cell stack size decreased in proportion to decreasing the fuel utilization. A one-dimensional fuel cell model was used to simulate the fuel cell while GateCycle® was used to simulate the performance of the associated recuperated turbine and various subsystems necessary for thermal management. For each test case, the size of the solid oxide fuel cell, gas turbine, and recuperator, as well as the fuel and air flow rates, hot-air bypass set point, and heat exchange effectiveness in the solid oxide fuel cell manifold were varied to obtain 550 MW_e output. In addition, anode recycle, turbomachinery efficiency, and various thermal management options were tested. The maximum system efficiency (75.6%) was attained for the single-pass solid oxide fuel cell with highly efficient turbomachinery when the solid oxide fuel cell used 80% of the incoming fuel. Efficiency was essentially flat from 75% fuel utilization through 85% fuel utilization. Employing anode recycle starting at 65% resulted in roughly 1 percentage point efficiency decrease for each percent increase in fuel utilization. For minimized solid oxide fuel cell degradation, a near 50:50 power split case was studied resulting in 68.6% efficiency and the solid oxide fuel cell using 55% of the incoming fuel. Because of shifting half of the power generation to the gas turbine, the size of the fuel cell stack was reduced by 25% as compared to that at maximum efficiency (80% fuel utilization).

1.0 Introduction

Solid oxide fuel cell (SOFC) - gas turbine (GT) hybrids show top electrical efficiencies around 70%, the highest of any power-cycle [1]. Efficiency and the types of fuel used in fuel-cells (e.g., syngas, reformed methane) combine to produce lower emissions than other fossil-powered technologies [2]. With this hybrid, high efficiency can be reached without the need for water cooling; therefore, water consumption per MW_e is lower than other technologies which approach the 70% efficiency mark. Integrated gasification SOFC-GT hybrid systems have higher power and better efficiency than integrated gasification combined cycle (IGCC) [3]. The impact of carbon capture and sequestration were also reported to be much lower for SOFC-GT than supercritical pulverized coal and IGCC [3] [4], even outperforming natural gas combined cycle (NGCC) [4]. High part-load efficiencies for turndown ratios up to 90% have been shown for these hybrids [5] [6] [7], which with the fuel flexibility of both SOFCs and GTs [5] [8] [9] [10], make this hybrid a robust fit for the evolving power-grid which is employing increasing numbers of generators that depend upon intermittent energy sources.

Issues which have prevented a large commercial market-share for the SOFC-GT hybrid include: high system-coupling and non-linear interactions [11], and the concomitant complexity of controls for the hybrid system, as well as the high expense and relative fragility (short working life) of fuel-cells. Work in the literature suggests that longer fuel cell lifetime can be achieved in hybrid systems at lower fuel utilization, directly impacting the economic viability of these systems [12].

Other researchers have looked at direct fired hybrid systems through parametric evaluation of performance criteria. Tarroja, et al. [13] developed a thermodynamic design space for a hybrid system operating on hydrogen, where the sizing of all components, except the fuel cell, were varied. They found that the highest fuel utilization is constrained by the heat requirement for the cathode. It was also shown that the penalty for operating the system at

[1] Corresponding author at: 3610 Collins Ferry Rd., Morgantown, WV 26507;
E-mail address: lshadl@netl.doe.gov (L. Shadle).

lower fuel utilization is substantial, and that the highest system efficiency is achieved at the highest feasible SOFC fuel utilization (U_f).

Based on an exergy analysis, Akkaya et al. [14] found that the highest system efficiency in a pressurized, direct-fired hybrid with steam bottoming occurs at 75% U_f. In this case, methane was used as the fuel, and like Tarroja et al., [13] the fuel cell size was fixed with its performance determined using a lumped model.

In another methane fueled direct hybrid, Yang, et al. [15] concluded that maximum hybrid efficiency is achieved when the SOFC-system outflow matches the desired turbine inlet temperature. Active temperature control of the cathode-inlet was found to have a detrimental effect on system efficiency. Fuel utilization was not varied in the study.

While incorporating thermal management methods for indirect natural gas reforming in a fuel cell turbine hybrid system, Haynes et al. [16] demonstrated that minimal change is observed in net efficiency with fuel utilization. Altering the U_f from 75% to 95% changes the system efficiency by less than 2 percentage points, implying tremendous flexibility in hybrid power systems.

Paramount to economic viability, cost factors other than efficiency must include size, flexibility, capital investment, and the share of power which each subsystem must provide, as well as their respective maintenance cycles over the service life. It is therefore essential to understand the interplay between subsystems of the SOFC-GT hybrid to find design criteria that will allow it to deliver highly efficient and flexible power at minimal cost.

Work in the literature has identified the promise of operating SOFC-GT hybrids at U_f lower than the maximum possible [14] [17] [18]. However, the optimal U_f was not identified. The previous work in the literature kept the size of the fuel-cell constant [13] [14] [15] [16] [17] [18], which may obscure the economic potential associated with varying the U_f of a hybrid system. The objective of this study is to identify the design SOFC U_f level which gives the highest lower heating value (LHV) efficiency for a SOFC-GT hybrid system while minimizing the installed costs.

The study described here uses a one-dimensional (1D) finite difference model of the fuel-cell. Temperature, current density, and fuel utilization are localized phenomena across the fuel cell, which are not resolved when using lumped averages for these values [10] [15] [19] [20] [21] [22] [23]. For example, peak temperatures and temperature gradients are reported to vary widely depending on whether the planar SOFC stack is operated in co-flow, counter-flow, or cross-flow configuration [21]. When an SOFC is simulated at high U_f, the current density profiles result in voltage calculations that are more accurate and yet substantially different from a lumped model result. Localized degradation must be considered to obtain accurate estimates of fuel-cell lifetimes [22]. Polarization losses are not accurately reflected using lumped models, but can be accurately captured in a 1D model [23]. In a lumped model, the temperature profile is assumed to be linear and first order, and in a distributed model with a more realistic temperature profile, heat transfer and the associated turbine performance, which relies on the heat flow from the fuel cell, can be dramatically different [10].

For the first time the impact of fuel-utilization on system performance is investigated in detail to design a direct fired hybrid plant while considering plant efficiency, equipment size, and thermal management including thermal gradients across the SOFC. Included in this study are analyses of anode-recycle, turbomachinery efficiencies, and gas bypass and heat-exchange alternatives. Results are also used to estimate capital costs associated with a given design, which largely depend on the power-share between fuel-cell and turbine. Ultimately, this study provides a basis for evaluating tradeoffs between optimum efficiency and economic viability.

2.0 Methods

A direct fired SOFC-GT hybrid cycle (Figure 1) was studied. Colors indicate purpose and/or state of the stream. Air serving the GT is blue; compressed/heated air serving the SOFC cathode is green; fuel is red; the post-SOFC (exhaust) stream which is expanded through the turbine is purple. Nominal conditions are presented in Table 1. In this cycle, ambient air (stream-1) is compressed to 4 atmospheres (stream-2) and heated through a recuperator (3) to serve as the SOFC cathode oxidant. A portion of this preheated air can be bypassed (4) to achieve the desired SOFC temperature, nominally 700°C. The heated, compressed air that is not bypassed enters the SOFC cathode via a manifold (5) where it may interact with heat from the SOFC-system's post-combustor. This manifold/post-combustor interaction is depicted in Figure 1 as SOFC Manifold Heat Exchange (HX) and stream 6,C is the resulting preheated flow stream fed into the cathode.

The fuel used in this study was a typical coal derived syngas (stream A) preheated to 800°C. The fuel flow to the anode (stream B) was equal to the fuel fed to the system when there was no anode recycle (AR) (stream G). AR is when the anode effluent is recycled through the anode again to achieve higher stack U_f while operating cells at a lower cell U_f. AR is commonly used to control carbon deposition when using methane fuel [16]. The impact of carbon deposition on the performance of SOFC were studied by Ma et al. [24]. While AR was not required for the methane free syngas used (Table 1), it was considered to evaluate its impact on hybrid performance. In those cases where AR was used, stream G dilutes the fuel being fed to the anode (B).

Air and syngas interact exothermically within the SOFC, generating electricity. The anode effluent (D) was combined with the cathode effluent (E) in the post combustor. This high temperature combustion exhaust (7,F) was used to preheat the incoming air in the cathode manifold when additional preheating of the SOFC was required.

The products of combustion in the SOFC manifold (8) were combined with any hot air diverted away from the SOFC (4) to form stream 9. After accounting for system pressure-drop this becomes the turbine inlet flow. These hot compressed products of combustion expand through the turbine (10) generating electricity and give up heat (in the recuperator) to newly compressed air before leaving system as process exhaust (11).

The study was conducted for a total system power fixed at 550 MW. The size is consistent with other Department of Energy (DOE) systems studies [25]. SOFC and GT cost are both driven by size. Thus, the power split impacted the equipment cost of each design. Unlike previous studies which varied only GT size, the SOFC size was also changed to accommodate their respective delivery requirements. Cells were added to the SOFC stack to obtain a given generation-capacity. By changing cell number, the total current was kept constant for a given stack, while changing the power-output of the fuel-cell system. The recuperator effectiveness and its area could vary to satisfy this parameter. The effectiveness of the manifold HX was varied between 0% and 50% to increase the cathode-inlet temperature desired in those cases requiring additional heat. The desired cathode air flow was achieved by varying both the compressor size and fraction of hot-air bypass.

General model – The scope of the two computer models used for this investigation is shown in Figure 1 – denoted as SOFC and GT under the process flow schematic. The SOFC model included the performance of the SOFC itself, as well as the post combustor. The GT model comprised the balance of the plant including the compressor, turbine, recuperator, hot-air bypass, as well as the SOFC manifold HX. The "chain-links" drawn in Figure 1 indicate where data were exchanged between the two models.

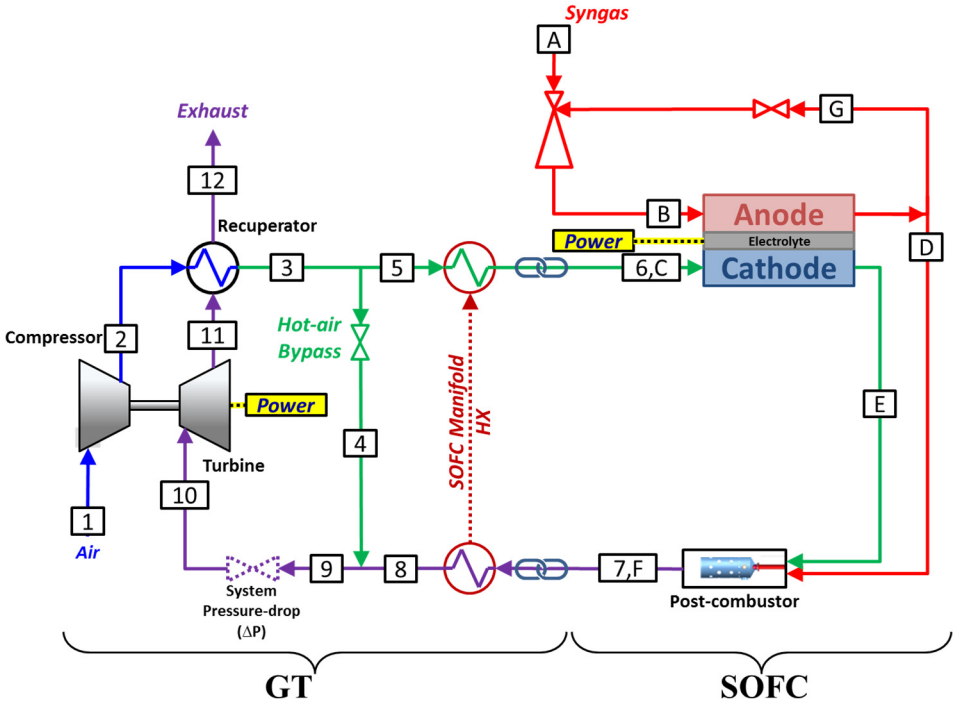

Figure 1: Process diagram of the SOFC-GT hybrid system.

The physical characteristics were kept constant at the cell level for the SOFC (Table 1). Efficiency characteristics were also kept constant at the process level in the GT. All components varied in size according to their required throughput. The baseline isentropic efficiencies for the turbomachinery were taken from a previously constructed model of the Mercury-50 turbine (a commercial recuperated machine), therefore the isentropic efficiencies of its turbomachinery (compressor and turbine) reflect those of the actual 5 MW_e machine.

Sensitivity studies – The impact of turbomachinery efficiencies and of AR were evaluated by a series of test simulations. In the former the compressor and turbine efficiencies were implemented at two levels over the entire range of U_f – one carrying over from the Mercury-50 model and one representing turbomachinery efficiencies expected

in a large-scale GT. The isentropic efficiencies of the large-scale equipment were taken as 90.5% for the compressor and 91.7% for the GT [26].

For the AR sensitivity study, cases above 65% U_f were simulated using both single-pass (SP) and various levels of AR to achieve comparable stack (global) fuel utilizations. All AR cases operated with 65% U_f at the cell. AR was increased incrementally to achieve stack fuel utilization of 70, 75, 80, 85, and 90%. Methods for calculating cell and stack fuel utilizations in the context of AR are described by Harun et al. [27].

Under thermal management, the requirement of 700°C for cathode-inlet temperature was relaxed. The hot-air bypass valve was closed and the cathode-inlet temperature was permitted to rise. This was implemented for U_f at 20, 50, and 70% to investigate an approach for decreasing losses associated with bypass operations. The impacts were evaluated on cathode-inlet temperature, system efficiency, and power split.

Table 1: Baseline SOFC-GT Hybrid Operating Parameters

SOFC System Parameters	
Current density	550 mA/cm^2
Initial fuel cell temperature	1,073 K
Cathode-inlet pressure	405 kPa
Cathode-inlet temperature	973 K
Fuel cell average solid temperature	1,108 K
Cathode-inlet composition: Air (vol. %)	O_2 21.0%, N_2 79.0%
Anode inlet pressure	405 kPa
Anode inlet temperature	1,073 K
Anode inlet composition: Syngas (vol. %)	CH_4 0.0%, CO_2 12.0%, CO 28.6%, H_2 29.1%, H_2O 27.1%, N_2 3.2%
SOFC Geometry	
Total cell area	200.0 x 200.0 mm
Anode thickness	0.5 mm
Electrolyte thickness	0.008 mm
Cathode thickness	0.05 mm
Oxidant/fuel channel size	2.0 x 2.0 mm
Number of oxidant/fuel channels	50
Number of fuel cell nodes (length)	20 (1 cm each)
GT System Parameters	
Pressure ratio	4
Compressor isentropic efficiency	83.6%
GT isentropic efficiency	87.0%
HX Parameters	
Effectiveness of GT recuperator	93.0%

Fuel cell model – The fuel was a coal-derived, methane-free syngas (Table 1). Therefore, fuel-reforming did not impact the results since the fuel processing unit was not considered in this study. Pressure loss across the SOFC and heat loss to the surroundings were assumed to be negligible. Included in the SOFC model was a post-combustor for unutilized fuel. Full details of the model development and validation are discussed in a publication by Hughes et al. [19].

The SOFC was simulated via a 1D model built in MATLAB®. The SOFC design was based on anode-supported, co-flow, and planar configuration, using stainless steel 441 (SS441) as the interconnects. The anode, cathode, and electrolyte, were composed of nickel-doped yttria-stabilized zirconia (Ni-YSZ), YSZ- lanthanum strontium magnetite (LSM), and YSZ, respectively.

The SOFC length was discretized using finite difference and finite volume difference to quantify the profiles of solid and air temperatures, local current density, Nernst potential, polarization losses, and fuel utilization. The cell voltage, V_{cell}, was calculated using Eq. 1-5.

$$V_{cell} = V_{Nernst} - \eta_{dif} - \eta_{act} - \eta_{ohm} \qquad (Eq.1)$$

$$V_{Nernst} = -\frac{\Delta G^{\circ}_{H_2O}}{2F} + \frac{R_u T}{2F} ln\left[\frac{p_{H_2}.p_{O_2}^{0.5}}{p_{H_2O}}\right] \qquad (Eq.2)$$

$$\eta_{dif} = \frac{R_u T}{2F}\left(ln\left(\frac{x_{H_2,bulk}.x_{H_2O,TPB}}{x_{H_2O,bulk}.x_{H_2,TPB}}\right) + \frac{1}{2} ln\left(\frac{x_{O_2,bulk}}{x_{O_2,TPB}}\right)\right) \qquad (Eq.3)$$

$$\eta_{act} = \frac{R_u T}{\alpha n F} sinh^{-1}\left(\frac{i}{2i_0}\right) \qquad (Eq.4)$$

$$\eta_{ohm} = ASR \cdot i \qquad (Eq.5)$$

The local current density, Nernst potential, and electrochemical losses across the fuel cell length changed in response to variations in composition and temperature distribution, assuming uniform voltage over the cell. In this model, only H_2 was considered as the active species for electrochemical oxidation.

Balance-of-plant model – Built in GateCycle®, this model included the recuperated turbine engine, HX at the cathode-inlet manifold, and total-system pressure-drop (shown as a purple valve in Figure 1). Pressure-drop developed in the hybrid system was a function of the amount of air routed through the hot-air bypass. This function, shown in Figure 2, was derived from experimental data at the National Energy Technology Laboratory's (NETL's) cyber-physical Hybrid Performance test facility.

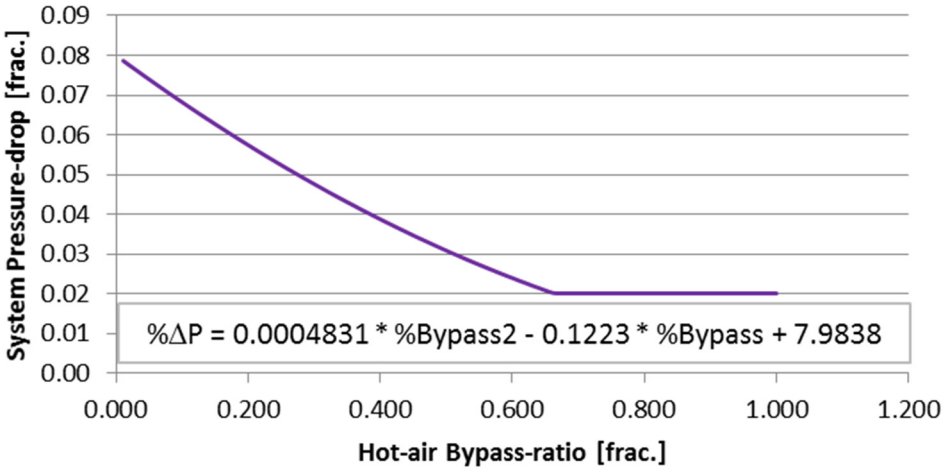

Figure 2: Pressure-drop function derived from test-stand results.

The maximum pressure-drop occurred when all the air entering the compressor passed through the fuel-cell (no air bypassing the SOFC). Minimum system pressure-drop was 2% of the total system pressure. HX at the cathode-inlet manifold was controlled by setting the HX-effectiveness to the minimum required to obtain the required cathode-inlet temperature. HX-effectiveness of the recuperator, however, was constant at 93%.

Model interactions – The order of calculations for the two models is shown in Figure 3, where, at "Start" a target or guessed SOFC power-output was specified with a given fuel utilization and a specified amount of AR. A solution for the SOFC model was then obtained using guessed flow rates and stack size (number of cells). The results were provided to the GT model and its solution was found by iterating to obtain a specified cathode-inlet temperature. If the GT and SOFC solutions did not provide the required total power, then the calculation was looped back to the top with new estimates for mass flow rate and stack size.

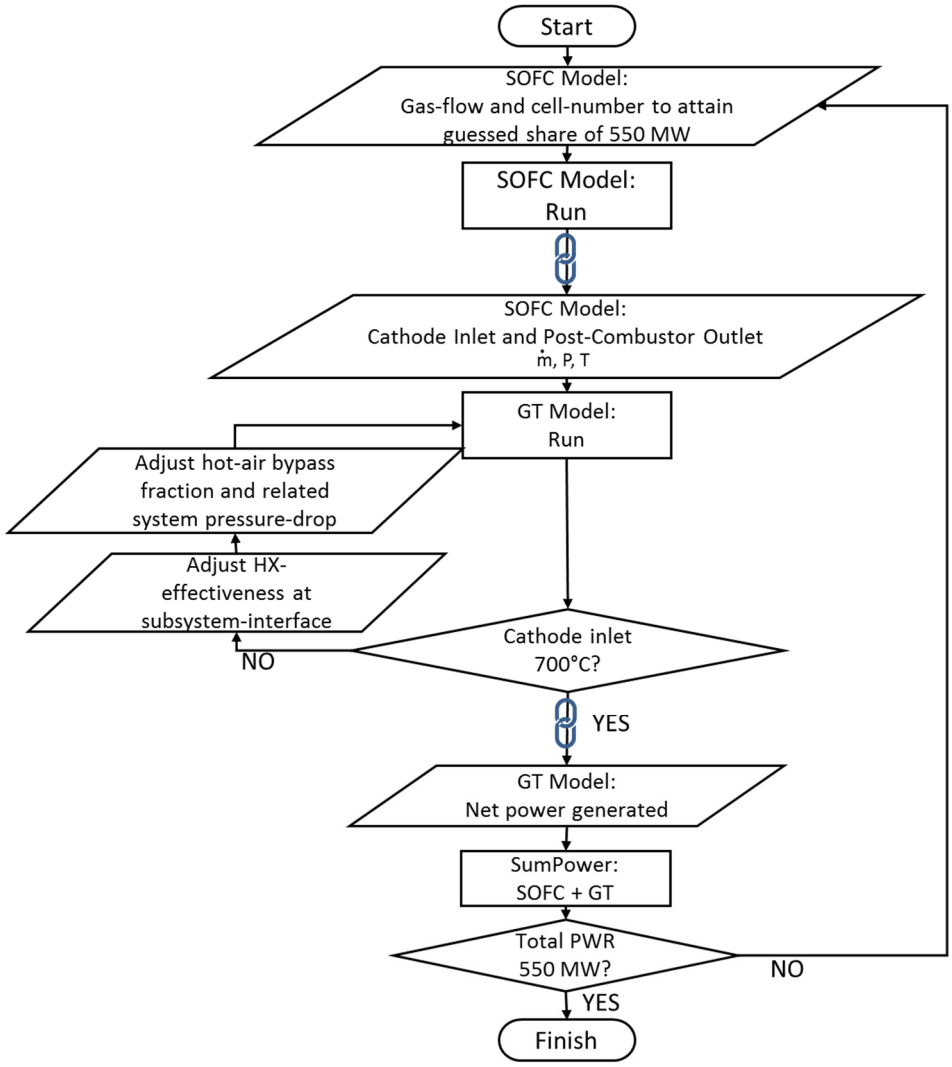

Figure 3: Calculation flow chart of SOFC and GT model execution.

Each case in this study was a separate hybrid system designed to attain 550 MW_e output with the SOFC operating at a given U_f. The trends compiled do not indicate behavior of a static system in response to changes in U_f.

Exergy loss – To identify mechanisms responsible for resultant system net efficiencies, exergy loss was evaluated at the: hot-air bypass; SOFC inlet manifold; pressure-drop process; compressor and turbine. Exergy loss is given as the exergy difference between high-availability and lower-availability states of the working-fluid. Fluid-exergy was evaluated using Eq. 6:

$$E_{fluid} = \dot{m}[(h_{station} - h_o) - T_o(s - s_o)] \qquad (Eq. 6)$$

Enthalpy and entropy were evaluated using REFPROP [28].

Cost – The system installed cost (C_{sys}) (including recuperated turbine and fuel-cell) was based on the equipment costs given by the Energy Information Administration [29] [30]. The Mercury-50 has a simple-cycle twin – the Centaur-50 – which was used in evaluating equipment costs for the various hybrid designs. The GT-recuperator cost, with respect to the rest of the GT, was scaled to match the 4% cost differential between the Solar Turbines simple-cycle Centaur-50 and recuperated-cycle Mercury-50 engines [31]. As the recuperator area scales with flow-rate for each hybrid case, the 4% cost differential was used for the recuperator in each design-case. The power delivered by each individual cell in the SOFC stack was the same for each design-case. Therefore, the SOFC cost was scaled by a constant factor ($/kW). The costing calculation is shown in Eq. 7.

$$C_{sys} = 1.04 C_{GT} PWR_{GT} + C_{SOFC} PWR_{SOFC} \qquad (Eq.\ 7)$$

C_{sys} is the sum of two products: GT subsystem cost per kilowatt and GT subsystem capacity; SOFC subsystem cost per kilowatt and SOFC subsystem capacity. Values for this study are as follows; C_{GT} = \$973/kW, C_{SOFC} = \$7,108/kW, PWR_{GT} = 142-483 MW, PWR_{SOFC} = 620-0407 MW. The cost of electricity (COE) is calculated by adding the sum of the operating cost and the cost of capital depreciation as described in Eq. 8:

$$COE = \frac{C_{sys}}{\beta \cdot Y \cdot P \cdot A} + \frac{C_{op}}{\gamma} \qquad (Eq.\ 8)$$

where, Y is the number of years over which the capital costs are depreciated, P is the production rate, A is the plant availability, C_{op} is the operating costs, β is the portion of capital costs that is attributed to major equipment, and γ is the portion of operating costs attributed to fuel costs. Plant depreciation was taken to be 10 years consistent with recent reports on the life expectancy for a SOFC in a hybrid configuration [12] [22]. The availability was assumed to be 90%. Values for β and γ were taken to be 0.6 and 0.8, respectively, based upon the relative contributions reported in NETL baseline studies for NGCC systems [25].

3.0 Results

The stream data for each case executed is compiled in Table 2. This table also shows the electric power generated by both subsystems in each case. The data for all cases using the baseline conditions is arranged in order of increasing U_f. The hybrid system efficiency increased with increasing U_f, maximizing at 80% U_f. Above 80% U_f the efficiency dropped off slightly (Figure 4). The hybrid efficiency at 65% and 90% U_f were nearly identical. As expected, the contribution of the SOFC to the total 550 MW_e output increased with increasing U_f. At peak system efficiency, the power split SOFC-GT was only 65%. A 50:50 power split was attained with a U_f of 55% corresponding to a drop of only 3 percentage points in efficiency.

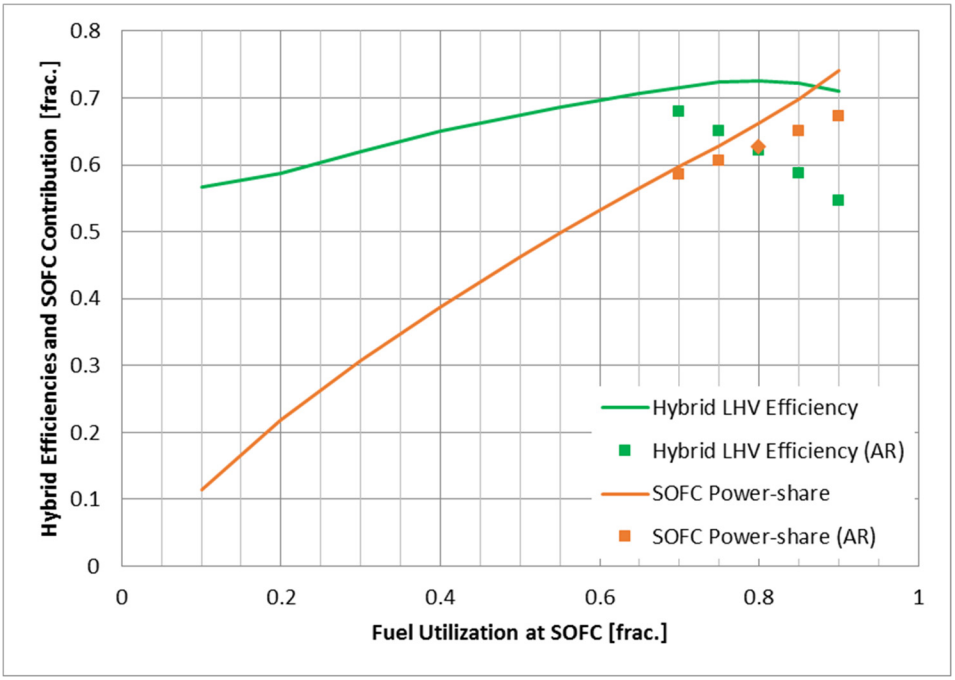

Figure 4: Hybrid system LHV efficiency; SOFC contribution to the total electrical power generated.

Increasing the efficiency of the turbomachinery increased the maximum hybrid electrical generating efficiency from 72.6 to 75.6%. The efficiency trend, with respect to U_f, were similar, but slightly less sensitive. The average improvement of the more efficient turbomachinery was to increase the hybrid electrical efficiencies by 3.5%. This increase was slightly larger at the very low levels of U_f and slightly smaller for the highest U_f values tested. The more efficient turbomachinery also resulted in a shift in the power split. The SOFC:GT power split was on the average 2.7 percentage points lower for the more efficient compressor-turbine pair. This effect was a bit more pronounced for

those cases relying on SOFC for power, i.e., with very high U_f and with AR, and less pronounced for cases dominated by the GT at the lowest levels of U_f.

Finally, employing AR to get to U_f levels higher than 65% reduced hybrid system efficiency. Employing AR did reduce the SOFC power contribution by as much as 10% at the highest U_f level and this would be accompanied by a similar reduction in SOFC size.

Two key factors influenced this set of results: exergy loss in various processes across hybrid cycle and changes in fuel-cell Nernst potential. In Figure 5, the electric power delivered to the power used is compared with that power used or rejected from the hybrid cycle. The power output by the SOFC continuously increased, while GT decreased with U_f, both varied in a non-linear manner. The compressor power was highest at very low and very high U_f, but power lost in the exhaust was highest at low U_f and decreased as U_f increased. The result was a minimum in exergy loss at 80% U_f. This comparison is analogous to calculating the fuel-efficiency ratio, and adds detail to the fate of the fuel-energy through a given design-case.

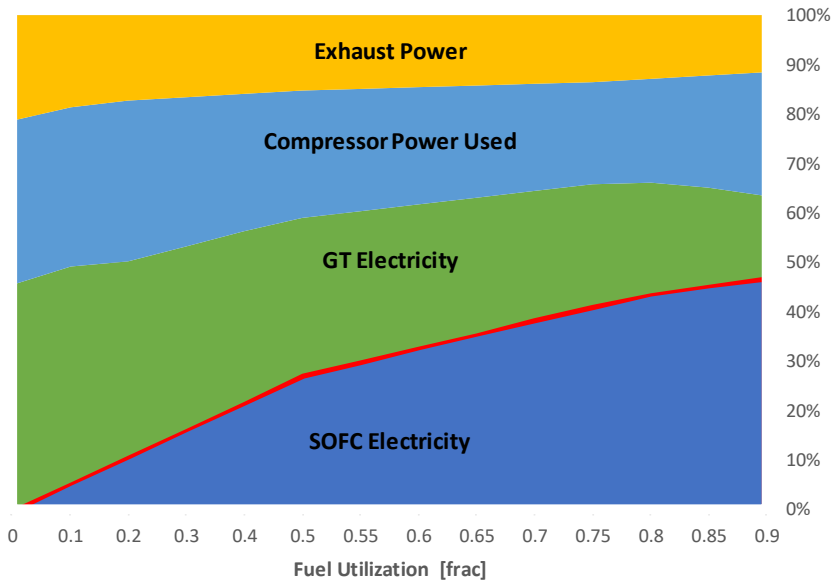

Figure 5: Power delivered by SOFC and GT as compared to parasitic power usage and power unrecovered from the hybrid cycle for baseline system varied over the entire U_f range.

Table 2: Summary Stream Table for All Baseline Cases Varying U_f and AR

Fuel utilization(U_f)			10%	20%	30%	40%	50%	55%	60%	65%	70%	70%	75%	75%	80%	80%	85%	85%	90%	90%
Anode recycle			No	No	No	No	No	No	No	No	No	Yes	No	Yes	No	Yes	No	Yes	No	Yes
1		[kg/s]	2129	2083	1841	1612	1414	1325	1241	1163	1088	1109	1019	1060	1025	1016	1127	1107	1270	1267
Air	T	[K]	288	288	288	288	288	288	288	288	288	288	288	288	288	288	288	288	288	288
	P	[kPa]	101	101	101	101	101	101	101	101	101	101	101	101	101	101	101	101	101	101
2		[kg/s]	2129	2129	1841	1612	1414	1325	1241	1163	1088	1109	1019	1060	1025	1016	1127	1107	1270	1267
Compressed Air	T	[K]	454	454	454	454	454	454	454	454	454	454	454	454	454	454	454	454	454	454
	P	[kPa]	405	405	405	405	405	405	405	405	405	405	405	405	405	405	405	405	405	405
4		[kg/s]	2534	1878	1466	1121	805	655	509	366	223	254	84	141	0	16	0	0	0	0
Hot Air Bypass	T	[K]	454	454	454	454	454	454	454	454	454	454	454	454	454	454	454	454	454	454
	P	[kPa]	405	405	405	405	405	405	405	405	405	405	405	405	405	405	405	405	405	405
5		[kg/s]	251	257	375	491	609	670	732	797	865	855	935	919	1025	1000	1127	1107	1270	1267
Compressed Hot Air	T	[K]	1029	973	973	973	973	973	973	973	973	973	972	973	935	973	850	903	763	826
	P	[kPa]	405	405	405	405	405	405	405	405	405	405	405	405	405	405	405	405	405	405
A		[kg/s]	125	121	115	110	106	104	103	101	100	105	99	110	99	115	99	122	100	131
Syngas	T	[K]	1073	1073	1073	1073	1073	1073	1073	1073	1073	1073	1073	1073	1073	1073	1073	1073	1073	1073
	P	[kPa]	405	405	405	405	405	405	405	405	405	406	405	406	405	407	405	407	405	406
B		[kg/s]	125	121	115	110	106	104	103	101	100	N/A	99	N/A	99	N/A	99	N/A	100	N/A
Anode Inlet	T	[K]	800	800	800	800	800	800	800	800	800	817	800	832	800	845	800	856	800	867
	P	[kPa]	405	405	405	405	405	405	405	405	405	406	405	406	405	407	405	407	405	406
6, C		[kg/s]	251	257	375	491	609	670	732	797	865	855	935	919	1025	1000	1127	1107	1270	1267
Cathode Inlet	T	[K]	1029	973	973	973	973	973	973	973	973	973	973	973	973	973	973	973	973	973
	P	[kPa]	405	405	405	405	405	405	405	405	405	405	405	405	405	405	405	405	405	405
D		[kg/s]	131	132	131	130	130	131	131	132	133	165	133	212	136	284	138	410	143	676
Anode Outlet	T	[K]	867	889	889	887	885	884	883	882	881	883	879	884	876	884	873	884	869	885
	P	[kPa]	405	405	405	405	405	405	405	405	405	406	405	406	405	407	405	407	405	406
E		[kg/s]	249	247	359	470	584	643	703	766	832	823	900	885	988	964	1088	1069	1228	1226
Cathode Outlet	T	[K]	863	887	887	885	884	883	882	880	879	881	877	882	875	882	872	882	868	882
	P	[kPa]	405	405	405	405	405	405	405	405	405	405	405	405	405	405	405	405	405	405
7, F		[kg/s]	375	378	490	601	715	774	835	898	965	960	1034	1029	1124	1115	1226	1229	1370	1398
Post Combustor	T	[K]	2703	2528	2114	1830	1627	1546	1475	1414	1359	1369	1310	1328	1267	1288	1229	1250	1192	1214
	P	[kPa]	405	405	405	405	405	405	405	405	405	405	405	405	405	405	405	405	405	405
G		[kg/s]	0	0	0	0	0	0	0	0	0	27	0	68	0	133	0	250	0	503
Anode Recycle	T	[K]	0	0	0	0	0	0	0	0	0	883	0	884	0	884	0	884	0	885
	P	[kPa]	0	0	0	0	0	0	0	0	0	406	0	406	0	407	0	407	0	406
8		[kg/s]	375	378	490	601	715	774	835	898	965	960	1034	1029	1124	1115	1226	1229	1370	1398
Final SOFC Exhaust	T	[K]	2703	2528	2114	1830	1626	1546	1475	1414	1358	1369	1310	1327	1235	1288	1124	1193	1012	1092
	P	[kPa]	405	405	405	405	405	405	405	405	405	405	405	405	405	405	405	405	405	405
9		[kg/s]	2253	2204	1956	1722	1520	1429	1343	1264	1188	1214	1118	1170	1124	1131	1226	1229	1370	1398
Mix with Bypass	T	[K]	1379	1305	1305	1304	1301	1299	1297	1294	1291	1292	1286	1443	1235	1284	1124	1193	1012	1671
	P	[kPa]	405	405	405	405	405	405	405	405	405	405	405	405	405	405	405	405	405	405
10		[kg/s]	2253	2204	1956	1722	1520	1429	1343	1264	1188	1214	1118	1170	1124	1131	1226	1229	1370	1398
Turbine Inlet	T	[K]	1106	1032	1032	1031	1028	1026	1024	1021	1018	1019	1013	1014	962	1010	851	920	739	819
	P	[kPa]	397	397	397	397	395	393	390	387	382	383	377	379	373	374	373	373	373	373
11		[kg/s]	2253	2204	1956	1722	1520	1429	1343	1264	1188	1214	1118	1170	1124	1131	1226	1229	1370	1398
Turbine Outlet	T	[K]	1070	1010	1010	1010	1010	1010	1010	1010	1010	1010	1009	1010	969	1010	878	936	786	852
	P	[kPa]	111	111	111	111	111	111	111	111	111	111	111	111	111	111	111	111	111	111
12		[kg/s]	2253	2204	1956	1722	1520	1429	1343	1264	1188	1214	1118	1170	1124	1131	1226	1229	1370	1398
Exhaust Gas	T	[K]	549	539	542	545	550	552	555	557	560	562	563	567	554	572	531	553	510	532
	P	[kPa]	111	111	111	111	111	111	111	111	111	111	111	111	111	111	111	111	111	111
SOFC		[MW]	62	120	169	213	254	274	293	312	330	323	345	333	365	345	384	358	407	371
GT		[MW]	484	427	380	336	295	276	257	239	221	228	204	217	186	206	166	193	142	180

The red line in Figure 5 indicates the efficiency of the SOFC subsystem. The SOFC efficiency increased with U_f, though the rate of increase was less for higher U_f. This "tailing off" is attributed to the drop in Nernst potential which accompanies high U_f. Below 75% U_f, the GT experienced little change in efficiency. The 10% U_f case used a higher SOFC cell temperature, which led to higher turbine-inlet temperature (T_{IT}) and resulting higher GT efficiency.

For several SP U_f cases, the working-fluid temperature history is plotted in Figure 6 for the hybrid using a SP SOFC over the full range of U_f. The abscissa shows stream locations matching Figure 1. From stream 3 to 6,C, heat is added at the SOFC manifold in preparation for entering the cathode. From the post combustor (7,F) to the turbine inlet (10), heat was transferred either via manifold HX or via hot-air bypass depending on the difference between post-combustor temperature and the cathode-inlet temperature requirement. Thus, peak temperatures at (7,F) resulted from additional heat generated by combusting unused fuel from the SOFC exhaust. The temperature changes from the post-combustor (7,F) to the turbine (10) are indicative of a loss in exergy for the fluid leaving the post-combustor. In cases designed for 20%-75% U_f, working-fluid temperature available for the turbine converged (streams 7,F to 10) and GT efficiency remained essentially constant over this range. By contrast as the design U_f was increased for 80% and above the turbine-inlet temperatures were progressively lower. This resulted in lower GT efficiency. The open circles in Figure 6 represent the temperatures in the GT operated in simple cycle, i.e., without any fuel being used by the SOFC. The converged T_{IT} for design-cases with U_f between 0.2 and 0.75 was only 5 K below the GT-only case.

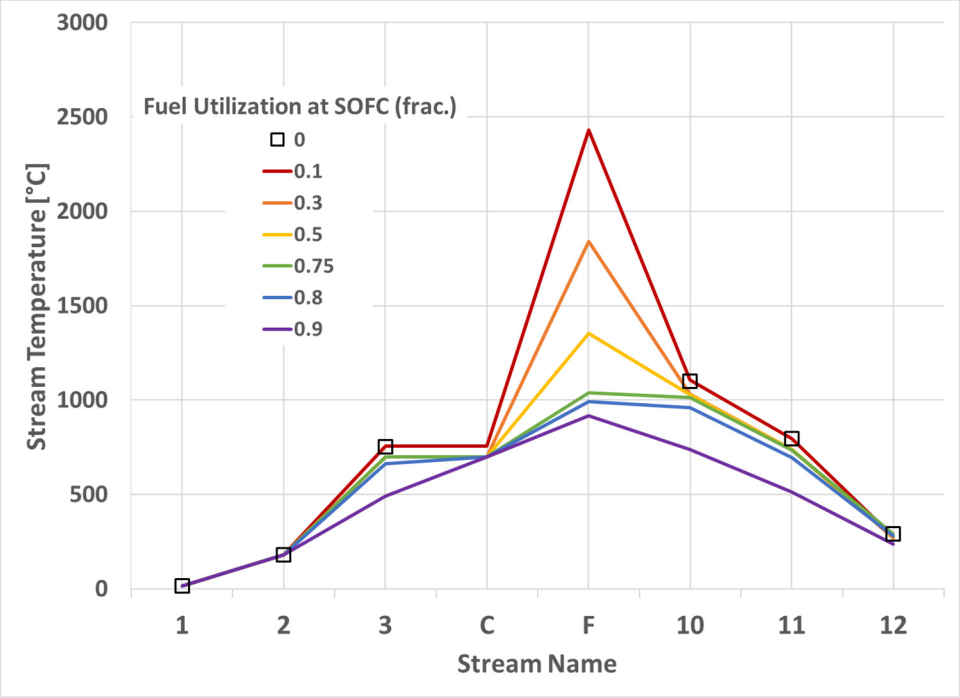

Figure 6: Temperature history of system working-fluid.

The additional combustion accompanying lower U_f may be expected to benefit the GT. However, at U_f below the optimum efficiency, temperatures from the post-combustor must be reduced to avoid excessive energy being recycled back to the cathode via the recuperator. This was accomplished using hot-air bypass. This practice caps the maximum turbine inlet temperature, and so the efficiency of the GT. The impact of U_f on the system becomes clearer when exergy-loss is evaluated.

Exergy loss results from frictional pressure loss, the mixing of flows at different temperatures, indirect transfer of heat from one fluid to another, or heat left unused in the system exhaust. The total exergy lost in each design-case is shown in Figure 7 with respect to the energy entering the system as fuel. In addition, the thermal exergy-loss contributions from processes composing the system are split out separately for each design-case in the color-coded column segments in Figure 7. The maximum efficiency (at 80% U_f) coincides with the minimum exergy-loss. Aside from exhaust losses, the heat-exchange processes were the most sensitive to U_f. Except for pressure-drop, all exergy-losing processes displayed a minimum around 80% U_f. The exergy loss for pressure-drop increased with increasing U_f. Loss via indirect heat exchange occurred at U_f >75% and grew with increasing U_f.

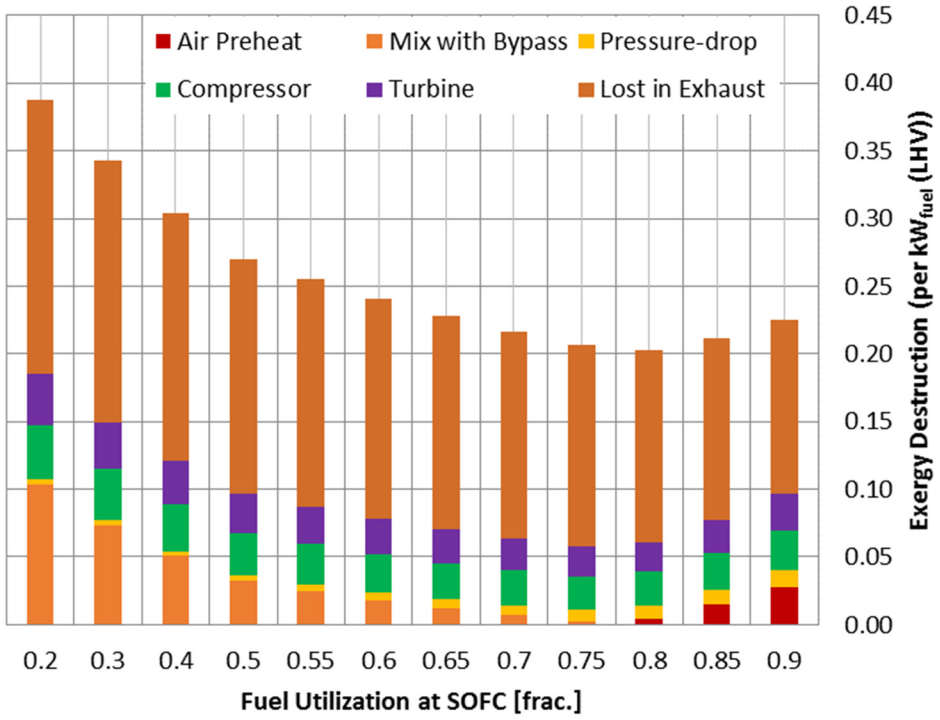

Figure 7: Contributors to total exergy loss.

The AR cases had generally lower efficiencies than the SP cases with the same U_f. The AR exergy-loss values were less sensitive to U_f than the AR efficiency values. This extra sensitivity can be attributed to a reduction in the Nernst potential associated with the anode-recycle process because of diluting the fuel being fed to the fuel cell.

The relationship between the Nernst potential across a given cell and U_f is shown in Figure 8. As U_f increased, the total Nernst potential of the cell decreased. This means the cell will produce less power for the fuel utilized by the SOFC, as indicated by Figure 5.

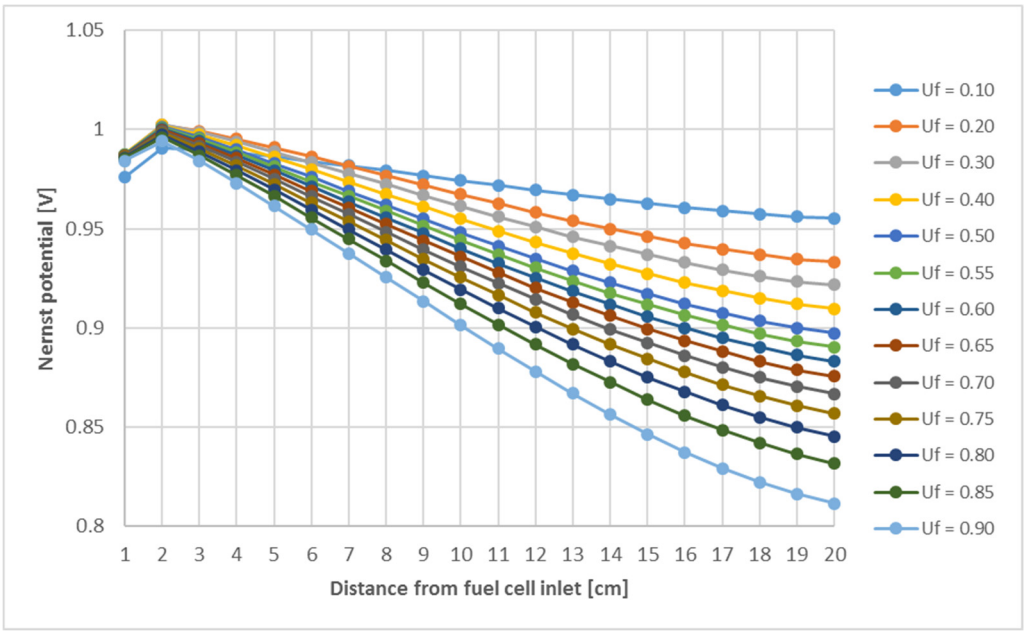

Figure 8: Nernst potential from cell entrance to exit.

The effect that U_f had on the sizes of the three major components of the hybrid is presented in Figure 9. The required number of cells in the SOFC increased and the GT capacity decreased in nearly linear fashion with increasing U_f. This was consistent with the increased power share from the SOFC with increasing U_f (Figure 4). Unlike SOFC and GT size, that recuperator size did not fall off monotonically with U_f, but instead began to rise for cases above 75% U_f. This curve correlated well with the compressor mass-flow (Figure 10), which also exhibited a minimum with U_f. At low levels of U_f, the compressor demand was high, but this dropped with increasing U_f as the amount of hot-air bypass was reduced because of the reduced cooling demand to moderate the cathode inlet temperature, T_{CI}. At U_f levels above 75% the compressor demand began to increase again to supply the increased demands by SOFC for cathode airflow and cooling. The 10% U_f case required a higher cathode-inlet temperature, so less compressor power was needed to achieve sufficient cooling via the hot-air bypass. This was a result of maintaining constant average temperature in the SOFC for all cases.

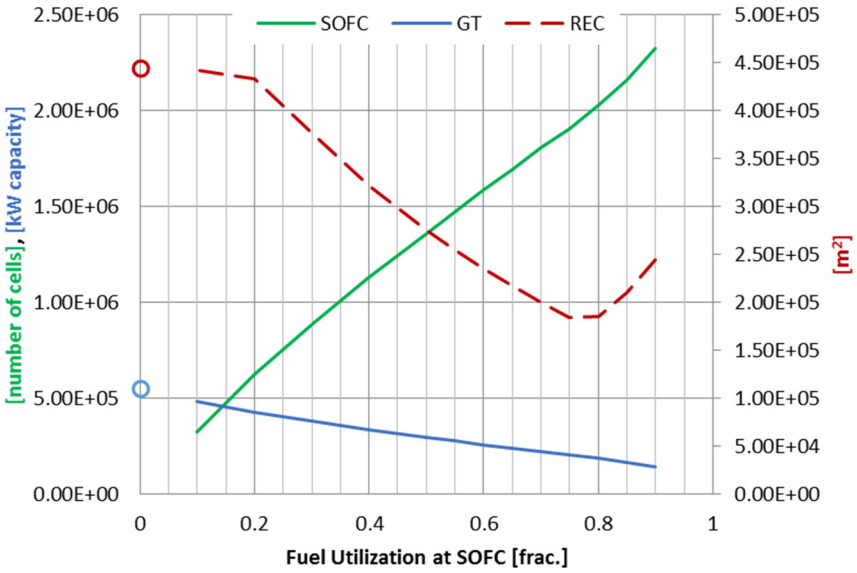

Figure 9: Component sizes for each design-case (the dashed curve refers to secondary axis).

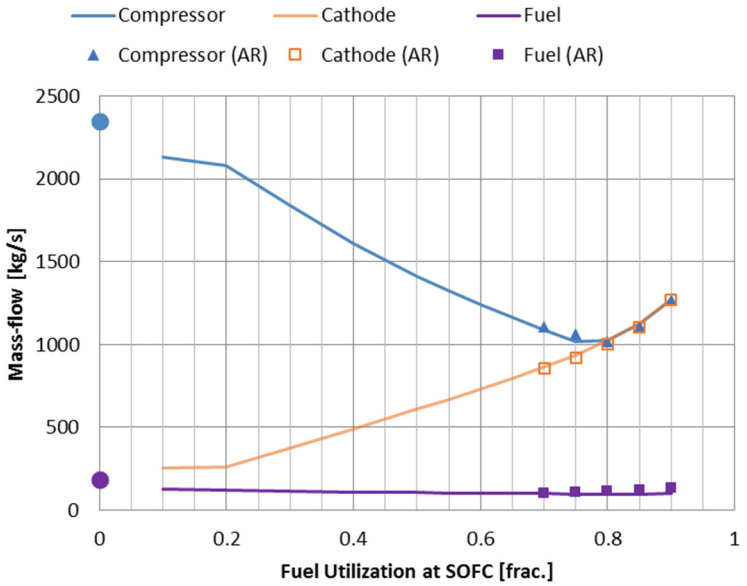

Figure 10: Inlet mass-flows to the SOFC-GT hybrid where filled circles represent the recuperated GT cycle and the other symbols represent the AR hybrid cases.

The component costs were scaled from the capacity of each of the power-systems in this hybrid. Noting the order of magnitude difference between the primary and secondary y-axes of Figure 11, costs of the SOFC dominated the cost of the hybrid system. The recuperator costs were estimated to be more than 2 orders of magnitude lower than the SOFC. The GT system costs were estimated to be a factor of 3 lower than the SOFC costs at 20% U_f when SOFC power share was approaching one-quarter of the hybrid. The cost ratio, SOFC:GT, was estimated to increase to 6:1 when the power share was equal. At optimum efficiency, U_f=80%, the cost ratio approached 10:1. For these reasons, the installed costs can be thought to be dictated by the fuel cell size.

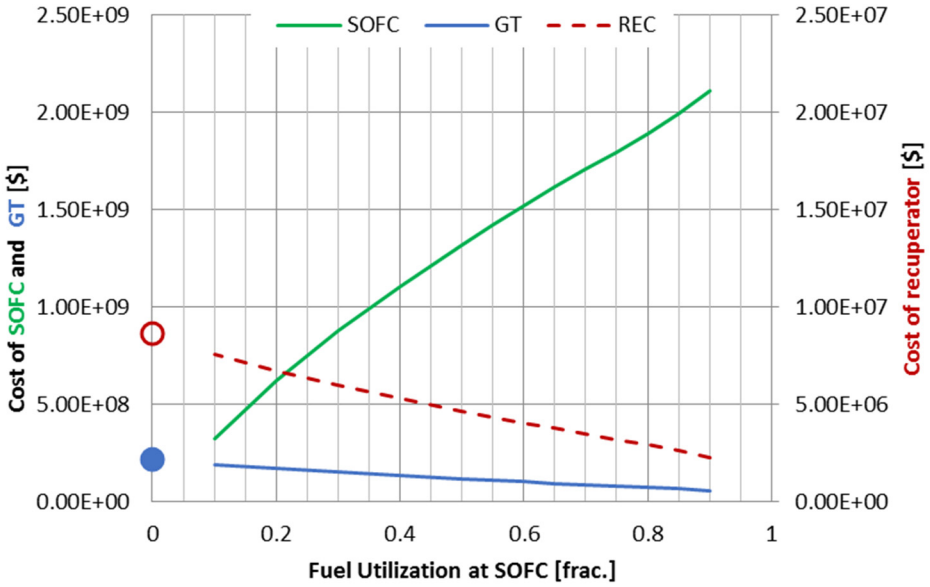

Figure 11: Equipment-only costs for major components of the SOFC-GT hybrid – SOFC, GT, Recuperator (the dashed curve refers to secondary axis).

Sensitivity – Three sensitivity studies were carried out to check the impact of assumptions made for this design-study. The assumptions investigated included: (1) setting a fixed, low HX-effectiveness at the subsystem-interface in the cathode manifold; (2) allowing a higher fuel cell temperature; (3) using more efficient turbomachinery. The differences in efficiency and power split compared to the base line tests (Table 2) are presented for several cases in each sensitivity study.

Table 3 gives these differences resulting from requiring a finite (5%) HX-effectiveness at the cathode-inlet manifold. The first three cases were SP with U_f <75%, in which the manifold effectiveness was limited to 5% rather than allowing it to drop to the 0% indicative of perfectly isolated streams. A slight drop in overall efficiency was observed which appeared to get larger as U_f was reduced. This was accompanied by a slight increase in the SOFC contribution. In the AR cases, the manifold HX was more integral to the thermal management system and fixing its effectiveness at 5% reduced heat transferred to the cathode, decreasing the cathode-inlet temperature thereby increasing the T_{IT}. As a result, hybrid efficiency increased and the SOFC power contribution reduced marginally for 70 and 75% U_f cases. In the 80% U_f cases, the difference in effectiveness was small and had correspondingly little impact on efficiency and power split.

Table 3: Impact of Requiring a Small, Given HX-Effectiveness (5%) at the SOFC-GT Interface

	Single Pass			*Anode Recycle*		
U_f *at SOFC*	*75%*	*70%*	*20%*	*80%*	*75%*	*70%*
Δ System Efficiency [% pt]	-0.18	-0.24	-2.66	-0.10	**0.86**	**0.57**
Δ SOFC Contribution [% pt]	0.20	0.18	0.97	0.13	**-0.75**	**-0.53**

The impact of raising the allowable cell-temperature to reduce the need for precooling cathode-inlet air is shown in Table 4. Increasing the allowable cathode-inlet temperature had a positive effect in the 20% U_f case. Like in the HX-effectiveness study, the impact of these changes was very small but increased with decreasing U_f.

Table 4: Impact of Closing Hot-Air Bypass and Allowing Higher Cathode-Inlet Temperature to Obviate Inlet Air Cooling

U_f at SOFC	70%	50%	20%
ΔT_{in} - Cathode [K]	25	68	79
Δ System Efficiency [% pt]	-0.13	-0.16	**1.88**
Δ SOFC Contribution [% pt]	0.18	0.36	**-0.62**

As the GT equipment becomes more efficient, the efficiency of the hybrid-system on this fuel increased as shown in Table 5. The average change in system efficiency was 3.5% increase with more advanced machinery and the power split shifted an average of 2.6% in favor of the GT. The only deviation from this was at 20% U_f, where the more efficient machinery produced a greater impact. The impact on power split however deviated from this average at both the extremes cases. At the highest U_f, the SOFC power contribution was reduced by 3% from the baseline case, while at the lowest U_f, the SOFC contribution was only reduced by 2% from its respective baseline case. Both results are inconsistent with the premise that hybrid performance always requires maximizing SOFC power share.

The optimum U_f remained the same for both sets of turbomachinery. Also, the impact of U_f decreased when more efficient turbomachinery was used. Thus, there was less of an efficiency drop-from-optimum in designing for a 50:50 power split as opposed to designing for the optimal efficiency. Increases in system efficiency found in each of these sensitivity investigations corresponded with decreases in the share of electricity produced at the SOFC.

Table 5: Impact of Higher-Efficiency Turbomachinery

	Single Pass							AR
U_f at SOFC	90%	85%	80%	75%	70%	65%	20%	90%
HE Net Efficiency	74.2	75.3	75.6	75.5	74.8	74.3	64.5	57.3
Δ System Efficiency [% pt]	3.20	3.05	3.00	3.22	3.29	3.65	5.77	2.63
Δ SOFC Contribution [% pt]	-3.18	-2.75	-2.61	-2.69	-2.63	-2.75	-2.01	-3.09

4.0 Discussion

The SOFC stack was simulated using a co-flow arrangement because computational fluid dynamic studies predict minimal thermal gradients compared to those using cross flow and counter-current flow arrangements. However, most fuel cell stacks are designed in cross flow configuration to simplify mechanical connections serving as the manifold into and out from the stack. The main conclusion regarding the impact of fuel utilization on efficiency and its remarkable insensitivity to the power split between the SOFC and the GT are expected to be unaffected by the flow configuration because these were design-studies such that the size of the turbine, recuperator, and fuel cell were adjusted to optimize performance. The thermal gradients were not found to be a limiting constraint in any of the cases as the fuel utilization was varied. However, when the flow arrangement is altered the thermal gradients will become greater and may become a limiting constraint requiring designs for additional thermal management.

The highest hybrid LHV-efficiency observed was 75.6%. This maximum occurred in the turbomachinery sensitivity study for the 80% U_f case using the more efficient GT as is consistent with the scale of this system. When less efficient turbomachinery was used in the baseline case, the peak hybrid efficiency was only 72.6% at the same U_f; however, the trends remained the same. Hybrid efficiency remained at high levels over a wide range of U_f. The efficiency at 90% U_f was the same as that attained at a U_f between 65% and 70%. The efficiency fell off gradually for both higher and lower U_f. The increases in SOFC's Nernst potential and GT's mass flow and T_{IT} have compensated for the reduced U_f and sustain high system efficiencies. This trend is consistent with other researchers also looking at the influence of U_f on similar hybrid systems, but running on methane and including reforming and AR. Akkaya et al. [14] found that exergy efficiency maximizes for 75%U_f and drops off gradually for both higher and lower levels of U_f. Haynes and Wepfer [16] found very little or no variation in SOFC-GT hybrid efficiencies over the range of 50 to 90% U_f.

Others have reported that hybrid performance is very sensitive to decreasing U_f. McLarty et al. [32] reported a 15% decrease in system efficiency when dropping from 80% to 60% U_f despite large increases in T_{IT}. However, they conducted their design analysis using a series of parametric tests in which the operating conditions were varied one at a time rather than designing an optimum system for each. While conducting the latter type of design analysis, it was often found that more than one parameter had to change to achieve the predefined operational targets and total power output. For example, both equipment sizes and flows were always altered as the U_f changed. In addition, their configuration used cathode recycle and recuperator bypass to achieve cathode flow and temperature requirements. These changes negatively affect the SOFC Nernst potential and exergy loss. The observed differences in sensitivity

can be attributed to these changes in design analysis, as well as to differences in operational and thermal management strategies.

Tarroja et al. [13] reported that system efficiency continuously increases with U_f when using H_2 for fuel. They noted, however, that for the cases above 80% U_f they were unable to manage the thermal demands of the SOFC and identify a practical constraint. In this study, a high HX-effectiveness at the cathode-inlet manifold was employed to obtain practical solutions for cases higher than 80% U_f, but the measures taken resulted in reduced system efficiencies. It has been recognized (e.g., [15] [9]) that some heat exchange could be designed into the cathode manifold between the post-combustor exhaust and the cathode air inlet. The effectiveness of that HX was expected to be low and was permitted to vary from 0% to 50%. As U_f increased above 80%, the effectiveness of HX increased reaching the 50% limit at 90% U_f. Cases attempted above 90% U_f did not produce practical solutions due to the similar constraints identified by Tarroja et al. [13]. The net result was a change in process efficiency which was less sensitive to changes in U_f, especially near the maximum efficiency.

Hybrid cycle analysis using methane as fuel found much lower system efficiencies, peaking at 66% [14] and 62% [16], compared to 75.6% reported here. These differences can be explained by differences in fuel, turbomachinery, and AR. The turbomachinery employed in both studies were consistent with a distributed microgrid and combined heat and power applications, rather than the high efficiency equipment employed in our sensitivity study. This would account for an additional 3-5 percentage point difference. A methane free syngas was used and energy costs to produce that fuel composition were not considered. This would include the heat of steam reforming methane and of heating it to the process temperature. The effect of this difference is not insignificant, but has not yet been established. The most significant difference was that the earlier studies evaluated systems with AR to control carbon deposition during on-cell reforming of methane. They used AR to control steam to carbon ratio of 2.5:1. This study found that AR resulted in a 5-15 percentage point reduction of efficiency depending on how much recycle was employed, principally due to the impact that AR has on fuel cell Nernst potential. The sensitivity to changes in U_f may be expected to vary depending on the level of U_f when AR is employed; however, neither of these studies report the level of AR nor the level of U_f based upon SP for the cell, only the net stack U_f.

McLarty et al. [32] reported an initial design system efficiency of 66% for coal syngas. This can be consistent with the results presented here of 75.6%, because the final optimized design performance would include the incremental influences of individual parameters such as U_f, P_r, T_{FC}, η_t, η_c. All of which are expected to increase their performance for an optimum design. In addition, some differences would be expected due to the differences in heat management and cathode recirculation described above.

Thermal Management – From the Exergy analysis, it was evident that the most efficient hybrid design appears to be one in which neither heating, nor cooling was required for the cathode-inlet flow at the cathode-inlet manifold. This is consistent with the conclusion of Yang et al. [15] that the optimum hybrid system is where turbine-inlet temperature matches the post-combustor-outlet temperature. This obviates bypass air, but also requires that the cathode-inlet and post-combustor outlet streams be thermally separated from each other. A sensitivity study was conducted to evaluate the impact of assuming a fixed, low HX-effectiveness at the subsystem-interface rather than allowing the effectiveness to vary. However, when it is necessary to operate a hybrid system at off design conditions, process controllers bypassing either hot or cold air around the fuel cell have been found to be highly efficient ways to follow load demands or make other necessary process state transitions.

The SOFC stack was simulated using a co-flow configuration which is reported to minimize thermal gradients compared to cross flow and counter-current flow planar fuel cell arrangements [21]. The thermal gradient across the solid phase in the SOFC using this 1-D model was constrained to 6°C/cm. During the analysis the SOFC was operated near this limit; only the highest U_f cases (>70%) without AR exhibited solids thermal gradients appreciably below this constraint approaching 5°C/cm at 90% U_f. As the U_f was reduced below 70% cases, progressively more hot air bypass was required to maintain the average SOFC operating temperature of 835 °C. Conversely, for the higher U_f cases, all the heat available from the recuperated compressor airstream was required and the maximum solids thermal gradient was still not attained. Currently, most fuel cell stacks are built using a cross flow configuration to simplify mechanical connections serving as the manifold into and out from the stack. The 1-D SOFC model does not permit the analysis of a cross flow SOFC configuration. Based upon the 3-dimensional computational fluid dynamic studies the localized thermal gradients will likely be larger for cross flow or counter flow configurations which will require changes be made to these thermal management systems. The effect should be similar to selecting a lower thermal gradient constraint or SOFC operating temperature.

Anode Recycle – For a methane-free syngas the AR was not required in cases below 70% U_f. Designing for recycle detracts from the efficiency readily attained in SP designs. As noted by Harun et al. from the same set of simulations, and shown by Figure 12 [27], "The recirculation of anode-off gas back into the inlet caused significant reduction in

the Nernst potential." This is attributed to a reduction in H_2 partial pressure. Therefore, the SOFC subsystem required more anode gas (fuel) flow to generate equivalent power.

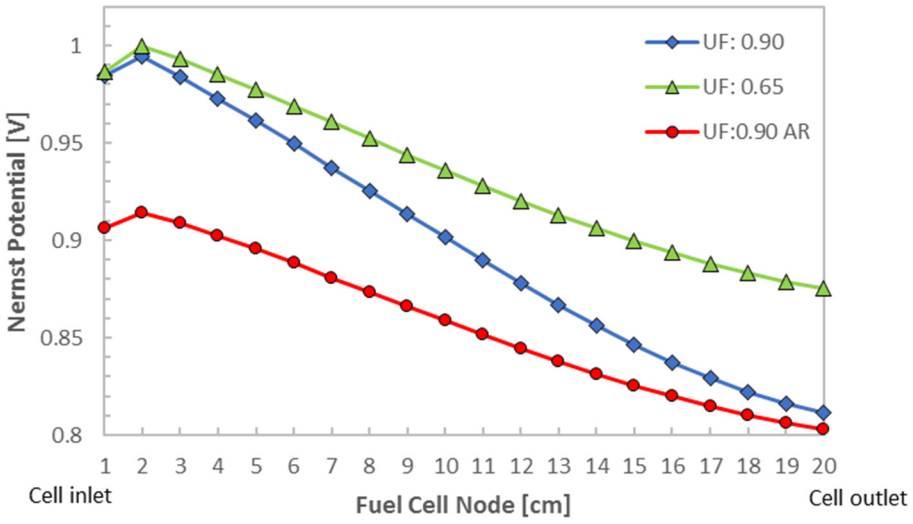

Figure 12: Comparison of Nernst potentials across a given cell.

Capital cost – Fuel utilization affected the share of power produced by each subsystem which in turn determined the size of each subsystem, and thereby the capital cost. This is evident if the shape of the SOFC-cost curve in Figure 11 is compared to the SOFC power-share curve in Figure 4. The magnitude of the SOFC cost in Figure 9 dominated that of the hybrid system.

Power split – At the maximum system efficiency, the power-share carried by the SOFC was found to be 63.6%. While the hybrid test facility at NETL was designed with the SOFC producing 60% of the power [33], it is typically operated with the SOFC producing nearly 90% of the power generated. Often, design-studies on SOFC-GT hybrids have not considered power split as a parameter [13] [15] [18] [9] [32]. Conventional practice has been to develop an SOFC-GT hybrid using an SOFC:GT power split of 80:20 [18] [14]. Li and Weng state simply that "In the SOFC-GT hybrid system, SOFC is the most important component that contributes most of the net power" [9]. McLarty et al. agree with Li and Weng, but state that "It is extremely likely that the optimal operating condition for a specific FC stack will be at lower fuel utilization when hybridized with a gas turbine" [32].

Because the efficiency of the SOFC, by itself, is higher than that of the GT, it is intuitive to expect that maximizing the power from fuel cell would provide the most efficient hybrid system efficiency. For this reason it is understandable that past researchers either did not report that the peak efficiency was found at low U_f [13], or reported only that peak efficiency occurred at low U_f and that low U_f reduced the SOFC power contribution [34], yet connected them together, and conclude that the highest efficiencies could be achieved with lower contributions from the SOFC.

Van Osdol et al. were the first to report that the U_f is the most sensitive parameter affecting the power split [17]. Others have reported that the exergy efficiency maximizes at 75% U_f [14], and that efficiency is constant over a range of U_f from 50%-80% [16]; however, these studies were operational parametric tests with fixed equipment size and without attempting to optimize the designs. Others fixed the U_f and varied the fuel composition [15] [9], GT equipment [13], or operating conditions in the SOFC [18] to evaluate performance impacts. None of the systems studies varied the SOFC size and the GT size to define the optimal hybrid configurations at each operating point.

This means that the configuration with the longest predicted life also uses a SOFC just over half the size of what would be required for a hybrid operating at maximum levels of U_f. In turn, the SOFC in a hybrid operating at a pressure ratio of 4 would be only one-half the size of the equivalent standalone SOFC.

Degradation of the SOFC has been reported to increase at lower temperature, higher current densities, and high U_f [22] [35] [36]. This current design-study was conducted by fixing the operating temperature, current density, and varying the U_f. However, it is recognized that during operations the SOFC will degrade. Since the degradation rate is reduced at lower U_f [27], one strategy would be to extend the life by changing U_f. As degradation proceeds the U_f can be reduced resulting in additional power being shifted to the turbine. For a hybrid designed for maximum efficiency the initial U_f was found to be 80% and the SOFC:GT power split was 65:35. As the hybrid plant ages the U_f would be

decreased in this off-design scenario until the hybrid achieves a 50:50 power split. Only a small decrease in efficiency would be expected if the GT and recuperator were slightly oversized to account for this degradation. Thus, the operating mode can be altered to optimize the power output and life expectancy to meet economic needs.

The design of a power system with a 50:50 power split and 55% U_f will extend the SOFC life while maintaining high efficiency (68%). Furthermore, it would require an SOFC of just over one-half the size of that required for a hybrid operating at maximum levels of U_f. In turn, the SOFC in a hybrid operating at a pressure ratio of 4 would be only one-half the size of the equivalent standalone atmospheric SOFC.

To optimize the power split, criteria must be established to evaluate the relative contributions of operating cleanly and efficiently with the initial capital investment. The contribution of equipment and efficiency to the COE were estimated using Eq. 8 and are presented in Figure 13. As the efficiency of the process increases the amount of fuel required to produce electricity decreases. The contribution of syngas fuel costs was assumed to be a constant value of 80% of the operating costs as is typical for natural gas fired power systems. Syngas costs were estimated to be twice that of natural gas used in NETL baseline studies [25]. The contribution of the operating costs to the COE exhibited a minimum of 63.6% for SOFC power. The major equipment costs were projected to be 80% of the total plant costs based upon the same baseline studies and were depreciated over 10 years based upon SOFC life expectancy [22]. The power plant was assumed to be available and operating 90% of the time. The contribution of these capital costs to the COE increased nearly linearly with SOFC power share for the hybrid system. The combined effect was a COE also displaying a broad minimum over a wide range. The COE was relatively constant for power splits with 40 to 60% SOFC contribution. If the fuel or equipment costs take on a greater share of the operating or lesser share of the capital expenses, respectively, then the power split favors the GT. Conversely, if the fuel or major equipment take on lesser share of the operating or greater share of the capital expenses, respectively, then the power split shifts in favor of the SOFC. Likewise, a SOFC lifetime shorter than 10 years favors a higher power contribution from the GT, while a longer life favors more SOFC power.

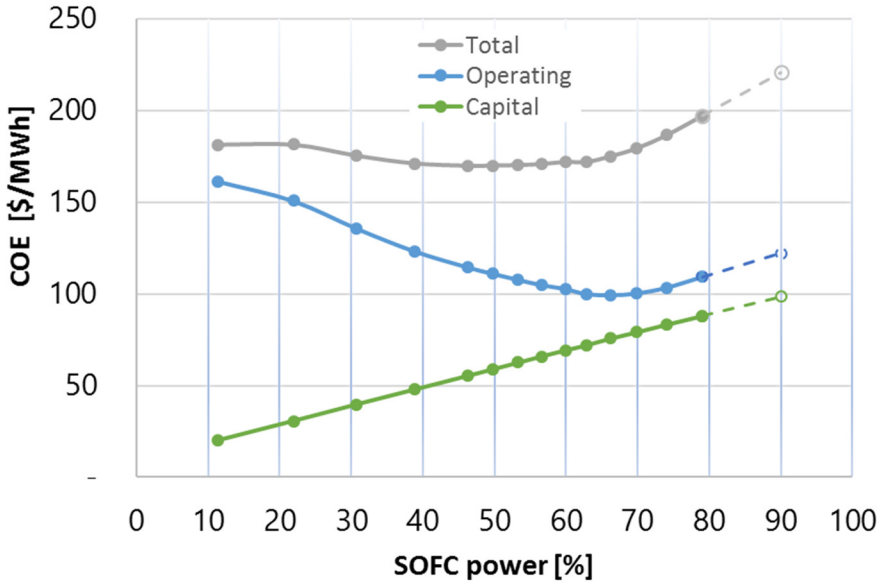

Figure 13: Cost of electricity (COE) for direct fired hybrid configuration fired on syngas as a function of the power split designed over the entire range of U_f studied. The dashed curve represents an extrapolation of the slopes between preceeding values.

5.0 Conclusions

This is the first ever design-study conducted on a direct fired solid oxide fuel cell-gas turbine hybrid to evaluate the optimal power split by varying fuel utilization. Plant designs for a wide range of fuel utilization were developed and the designs evaluated considering efficiency, equipment size, and realistic thermal management systems. Unlike previous systems analyses, a one-dimensional fuel cell model was used to capture localized effects which impact system performance parameters to achieve greater accuracy than a lumped model approach. In this way design cases were achieved with the constraints of solid oxide fuel cell operational temperatures and thermal gradients. The optimal system efficiency was found in a design which avoided active temperature-control of the cathode-inlet stream (by heat

exchange at the cathode-inlet manifold, or hot-air bypass). The net system efficiency reached a maximum of 75.6% at 80% fuel utilization for the single pass configuration with a resulting power split of 66.2% fuel cell to 33.8% turbine.

The hybrid performance was fairly level near the maximum value– that is, the influence of fuel utilization and power split on efficiency was small near this maximum. The hybrid with 50% power from the solid oxide fuel cell had the same efficiency as the hybrid with 80% power from the solid oxide fuel cell. Likewise, efficiencies were the same at fuel utilization of 55% and 90%.

The hybrid performance was even less sensitive to changes in fuel utilization with more efficient turbomachinery. The net system efficiency of 72.3% occurred at 75% fuel utilization; and at 85% fuel utilization the system was 72.2% efficient. More efficient turbomachinery decreased the power contribution which must be made by the solid oxide fuel cell.

The solid oxide fuel cell performance was negatively affected at higher levels of fuel utilization and by anode recycle. The solid oxide fuel cell Nernst potential was reduced by increasing fuel utilization and it was strongly degraded by anode recycle. Adding anode recycle for syngas resulted in large reductions in system efficiency. With anode recycle the system efficiency was 62.1% at 80% fuel utilization, a 10.5 percentage point drop compared to no anode recycle. This is dramatic considering that the single pass efficiency at 65% fuel utilization was 70.7%, only 1.9 percentage points less than the optimal efficiency at a fuel utilization of 80%. Anode recycle is not recommended for the hybrid configuration studied.

A target design with a 50:50 power split was considered to maximize operational flexibility, fuel-cell lifetime, and equipment cost savings. This design point was found to be 68.6% efficiency with a fuel utilization of 55% and had a hybrid installed cost which was four-fifths that of the 80% fuel utilization case.

The hybrid system shows a performance optimum at solid oxide fuel cell fuel-utilizations less than the theoretical maximum for a standalone solid oxide fuel cell. Therefore, hybridizing allows less extreme fuel-cell design. As observed by others, by generating power from solid oxide fuel cell-stack exhaust, the electrical efficiency of the hybrid generally exceeds that of either the solid oxide fuel cell or gas turbine alone. This leads to the conclusion that the most cost-effective and efficient deployment of a solid oxide fuel cell would be in a solid oxide fuel cell-gas turbine hybrid, as both fuel-cost and stack-replacement can be minimized via this hybridization, though the comparative cost of control systems may reduce this benefit. Noting that optimum efficiency is reached at lower solid oxide fuel cell:gas turbine power splits, an opportunity is recognized for earlier adoption of fuel-cell power-production. This is because the fuel-cell need not be so large, and because it can be operated in a manner less stressful on its materials – mitigating the risk of buying and breaking a fuel-cell.

DISCLAIMER

ACKNOWLEDGEMENT

This work was funded by the U.S. Department of Energy (DOE) Crosscutting Research program, implemented through the Technology Development & Integration Center (TD&IC), Coal, in the Office of Fossil Energy (FE).

NOMENCLATURE

1D	One-dimensional
A	Plant availability (%)
AR	Anode recycle
CMP	Compressor
COE	Cost of electricity
DOE	Department of Energy
FE	Fossil Energy
GT	Gas turbine
IGCC	Integrated gasification combined cycle
LHV	Lower heating value [kJ/kg]

LSM	Lanthanum strontium magnetite
NETL	National Energy Technology Laboratory
NGCC	Natural gas combined cycle
Ni-YSZ	Nickel-doped yttria-stabilized zirconia
P	Production rate [MWh/yr]
SOFC	Solid oxide fuel cell
SP	Single-pass
TD&IC	Technology Development & Integration Center
YSZ	Yttria-stabilized zirconia
ASR	Area specific resistance [Ω-m^2]
U_f	Fuel utilization by SOFC (%)
C	Cost [$]
C_{sys}	System installed cost [$]
E	Exergy [kW]
F	Faraday's constant [C/mol]
α	Charge transfer coefficient
β	Fraction of capital costs attributed to major equipment
γ	Fraction of operating costs attributed to fuel
h	Specific enthalpy [kJ/kg]
i	Current density [mA/cm^2]
i_0	Exchange current density [A/cm^2]
$\dot{m}$	Mass flow [kg/s]
n	Number of electrons transfer per reaction
η	Electrochemical loss [V]
p	Partial pressure [atm]
P_r	Pressure ratio
η_t,	Turbine isentropic efficiency [%]
η_c	Compressor isentropic efficiency [%]
R_u	Ideal gas constant [8.314 J/mol-K]
s	Specific entropy [kJ/kg-K]
T	Temperature [K]
V_{cell}	Cell voltage, overpotential [V]
V_{Nernst}	Nernst potential [V]
x	Mole fraction
Y	Depreciation time [years]
ΔG°	Standard Gibbs free energy [kJ]
ΔP	Pressure differential [kPa]

SUBSCRIPTS

0	Dead state
c	Compressor
CI	Cathode inlet
FC	Pertaining to the Fuel Cell
IT	Turbine inlet
t	Turbine
TPB	Triple phase boundary
bulk	Anode/cathode stream
act	Activation
dif	Diffusion
ohm	Ohmic

REFERENCES

[1] S. J. McPhail, L. Leto and C. Boigues-Munoz, Yellow Pages of SOFC Technology, Rome, Italy: ENEA, National Agency for New Technologies, Energy and Sustainable Economic Development, 2012-2013.

[2] Y. Welaya, M. Mosleh and N. Ammar, "Thermodynamic analysis of a combined gas turbine power plant with a solid oxide fuel cell for marine applications," *Int. J. Nav. Archit. Ocean Eng.,* pp. 529-545, 2013.

[3] S. Park, J. Ahn and T. Kim, "Performance evaluation of integrated gasification solid oxide fuel cell/gas turbine systems including carbon dioxide capture," *Applied Energy,* vol. 88, p. 2976–2987, 2011.

[4] J. Nease and T. Adams, "Comparative life cycle analyses of bulk-scale coal-fueled solid oxide fuel cell power plants," *Applied Energy,* vol. 150, p. 161–175, 2015.

[5] D. Tucker, C. Haynes and P. Geoghegan, "Needs and Approaches for Novel Characterization of Direct Hybrid Fuel Cell/Gas Turbines," in *Proceedings of the ASME 2015 Power and Energy Conversion Conference*, San Diego, California, U.S.A., 2015.

[6] F. Trasino, M. Bozzolo, L. Magistri and A. Massardo, "Modeling and performance analysis of the Rolls-Royce Fuel Cell Systems Limited 1 MW plant," *Journal of Engineering Gas Turbines Power,* vol. 133, no. 59328, 2011.

[7] L. Barelli, G. Bidini and A. Ottaviano, "Part load operation of a SOFC/GT hybrid system: Dynamic analysis," *Applied Energy,* vol. 110, p. 173–189, 2013.

[8] N. Harun, Fuel composition transients in solid oxide fuel cell gas turbine hybrid systems for polygeneration application, Hamilton, Ontario: PhD Disertation at McMaster University, 2015, p. 155.

[9] Y. Li and Y. Weng, "Performance study of a solid oxide fuel cell and gas turbine hybrid system designed for methane operating with non-designed fuels," *Journal of Power Sources,* vol. 196, p. 3824–3835, 2011.

[10] N. Harun, D. Tucker and T. Adams, "Technical challenges in operating an SOFC in fuel flexible gas turbine hybrid systems: Coupling effects of cathode air mass flow," *Applied Energy,* vol. 190, p. 852–867, 2017.

[11] P. Pezzini, S. Celestin and D. Tucker, "Control Impacts of Cold-Air Bypass on Pressurized Fuel Cell Turbine Hybrids," *Journal of Fuel Cell Science and Technology,* vol. 12, no. 1, pp. 011006: 1-8, 2015.

[12] F. Harun, V. Zaccaria, D. Tucker, A. Traverso and T. Adams II, "Degradation Analysis of SOFC for Various Syngas Compositions in IGFC Systems," in *International Gas Turbine Congress 2015, November 2015, Paper N. 38.*, Tokyo, Japan, 2015.

[13] B. Tarroja, F. Mueller, J. Maclay and J. Brouwer, "Parametric Analusis of a Solid Oxide Fuel Cell Gas Turbine Design Space," *Journal of Engineering for Gas Turbines and power,* vol. 132, no. July, pp. 072301:1-11, 2010.

[14] A. Akkaya, B. Sahin and E. H. Huseyin, "An analysis of SOFC/GT CHP system," *Int. J Hydrogen Energy,* vol. 33, no. 10, p. 2566–2577, 2008.

[15] W. Yang, S. Park, T. Kim, J. Sohn and S. Ro, "Design performance analysis of pressurized solid oxide fuel cell / gas turbine hybrid systems concerning temperature constraints," *Journal of Power Sources,* vol. 160, pp. 462-473, 2006.

[16] C. Haynes and W. Wepfer, "Enhancing Fuel Cell / Gas Turbine Performance via Reduced Fuel Utilization within Indirect Internally Reforming (IRR) Fuel Cell Stacks," in *Proceedings of ASME International Meeting of Early Career Engineers (ICEME)*, Atlanta, GA, 2000.

[17] J. VanOsdol, E. Liese, D. Tucker, R. Gemmen and R. James, "Scaling a Solid Oxide Fuel Cell Gas Turbine Hybrid System to Meet a Range of Power Demand," *Journal of Fuel Cell Science and Technology,* vol. 7, no. FEBRUARY, pp. 0150011-0150018, 2010.

[18] P. Costamagna, L. Magistri and A. Massardo, "Design and part-load performance of a hybrid system based on a solid oxide fuel cell reactor and a micro gas turbine," *Journal of Power Sources,* vol. 96, pp. 352-368, 2001.

[19] D. Hughes, W. Wepfer, K. Davies, J. C. Ford, C. Haynes and D. Tucker, "A robust, real-time, distributed solid oxide fuel cell model for hardware-based simulation of integrated hybrid systems," in *Proceedings of ASME 2011 9th Fuel Cell Science, Engineering and Technology Conference, ESFuelCell2011,*, Washington, DC, 2011.

[20] D. Cheddie and N. Munroe, "Dynamic 1D model of a solid oxide fuel cell," *Journal of Power Sources,* vol. 171, p. 634–643, 2007.

[21] E. Achenbach, "Three-dimensional and time-dependent simulation of a planar solid oxide fuel cell stack," *Journal of Power Sources,* vol. 49, pp. 333-348, 1994.

[22] V. Zaccaria, D. Tucker and A. Traverso, "Operating strategies to minimize degradation in fuel cell gas turbine hybrids," *Applied Energy,* pp. 437-445, 25 October 2016.

[23] M. Sorrentino, C. Pianese and Y. G. Guezennec, "Hierarchical modeling approach to the simulation and control of planar solid oxide fuel cells," *Journal of Power Sources,* vol. 180, p. 380–392, 2008.

[24] T. Ma, M. Yan, M. Zeng, J. Yuan, Q. Chen, B. Sundén and Q. Wang, "Parameter study of transient carbon deposition effect on the performance of a planar solid oxide fuel cell," *Applied Energy,* vol. 152, p. 217–228, 2015.

[25] T. Fout, A. Zoelle, D. Keairns, M. Turner, M. Woods, N. Kuehn, V. Shah, V. Chou and L. Pinkerton, "Cost and Performance Baseline for Fossil Energy Plants Volume 1a: Bituminous Coal (PC) and Natural Gas to Electricity Revision 3," DOE/NETL-2015/1723, Morgantown, WV, 2015.

[26] J. Black, V. Chou, D. Keairns, M. Turner, M. Woods and A. Zoelle, "Process Modeling Design Parameters; Quality Guidelines for Energy Systems Studies," DOE/NETL-2014/051314, Morgantown, WV, 2014.

[27] F. Harun, L. Shadle, D. Oryshchyn and D. Tucker, "Fuel Utilization Effects on System Efficiency and Solid Oxide Fuel Cell Performance in Gas Turbine Hybrid Systems," in *Proceedings of ASME Turbo Expo 2017: Power for Land, Sea and Air GT2017-64055*, Charlotte, NC., 2017.

[28] E. Lemmon, *REFPROP 9.0,* NIST.

[29] Independent Statistics and Analysis, EIA, "Updated Capital Cost Estimates for Utility Scale Electricity Generating Plants," April 2013. [Online]. Available: www.eia.gov/outlooks/capitalcost/pdf/updated_capcost.pdf.

[30] United States Department of Energy, "U.S. Energy Information Administration," April 2013. [Online]. Available: www.eia.gov/outlooks/capitalcost/pdf/updated_capcost.pdf.

[31] Gas Turbine World, "Simple Cycle," *Gas turbine World Handbook,* 2010.

[32] D. McLarty, J. Brouwer and S. Samuelsen, "Hybrid Fuel Cell Gas Turbine System Design and Optimization," *Journal of Fuel Cell Science and Technology,* vol. 10, pp. 041005:1-11, AUGUST 2013.

[33] D. Tucker, E. A. Liese, J. VanOsdol, L. O. Lawson and R. S. Gemmen, "Fuel Cell Turbine Hybrid Simulation Design Facility," in *Proceedings of the ASME, Int. Mechanical Eng. Congress and Expo, IMECE2002-33207*, New Orleans, LA, 2002.

[34] W. Winkler, P. Nehter, M. C. Williams, D. Tucker and R. Gemmen, "General fuel cell hybrid synergies and hybrid system testing status," *Journal of Power Sources,* vol. 159, p. 656–666, 2006.

[35] A. Hagen, R. Barfod and P. Hendriksen, "Degradation of anode supported SOFCs as a function of temperature and current load," *J Electrochem Soc,* vol. 153, p. 165–171, 2006.

[36] A. Nakajo, F. Mueller, J. Brouwer, J. van Herle and D. Favrat, "Progressive activation of degradation processes in solid oxide fuel cells stacks: Part I: Lifetime extension by optimisation of the operating conditions," *J Power Sources,* vol. 216, p. 449–463, 2012.